Preliminary Design of a Mechanical Differential and Test Bench for a P4 Hybrid Electric Pickup

Aldo Silva Gonçalves
Automotive Technology Residency Program, Universidade Federal de Pernambuco, Recife, Brasil

Alexandre da Silva Scari
Graduate Program in Mechanical Engineering, Universidade Federal de Minas Gerais, Belo Horizonte, Brasil

ABSTRACT

This work presents the mechanical design of a rear axle electric powertrain for a P4 hybrid electric mid-size pickup truck, along with the preliminary design of a test bench for system evaluation. The study includes the design and dimensioning of all differential gears according to the AGMA standard, the analysis of the half shafts and splines, and the selection of appropriate bearings. Additionally, a conceptual and preliminary test bench design is proposed, enabling the simulation and testing of P4 parallel hybrid electric vehicle (HEV) operation under different control strategies. This approach allows for the manufacturing and validation of all components within the proposed system.

Keywords: Hybrid vehicles. Mid-size pickup trucks. Mechanical differential. Test bench. off-road vehicles.

INTRODUCTION

The automotive market has experienced significant transformation in recent years. According to the Brazilian Association of Electric Vehicles (ABVE), the number of hybrid vehicle (HEV) sales in 2024 increased by 55.1% compared to 2023, accounting for 65% of the total electrified vehicles in Brazil. Among them, the majority (36%) consists of plug-in hybrids (PHEV) [1]. This trend is also observed in other emerging countries, such as India [2].

One of the reasons for this transformation is the arrival of Chinese automakers in the country, particularly BYD and GWM, which have introduced highly technological vehicles at competitive prices and are already planning to manufacture their cars domestically [3], [4]. Of the ten best-selling electrified models in Brazil, five are Chinese. Furthermore, increasingly stringent public policies are being implemented to limit pollutant emissions, such as PROCONVE L8 in Brazil [5].

In this scenario, there are several possible hybridization architectures. One less explored commercially is the P4, which consists of an electric motor (EM) coupled to a mechanical differential on the vehicle's rear axle, enabling eAWD capabilities. This configuration is suitable for pickup trucks, as it allows off-road characteristics without needing a robust internal combustion engine (ICE) and a driveshaft. The P4 architecture features a simpler integration effort due to its independence from the existing powertrain. The eAWD system can also add more safety and can be cheaper than the P2 [6]. Furthermore, currently, no hybrid pickup trucks are produced in Brazil. The definition of hybrid topologies is shown in Figure 1.

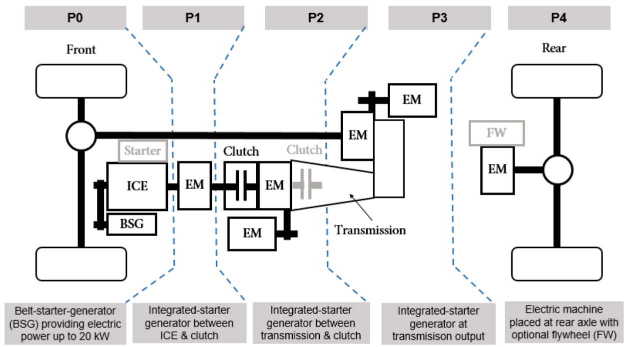

Figure 1 – Different hybrid topologies. Adapted from [6].

Although there are many papers in this field, most of them focus on modeling simulation studies [7], [8], [9]. According to Hui et al. HEVs are very complex systems, difficult to accurately mathematically model or describe, and the validation of simulation results should be proved by other methods [10]. In this context, it is important to build a real system and test it on a bench. Sitting et al. present a new approach combining strategies for PC simulations and a hybrid powertrain test bench during the development of HEVs [11]. Another interesting study consists of a versatile test bench, capable of fulfilling operational tests of series and parallel HEVs [10]. None of them approach the mechanical design of the electric powertrain and the selection of the components, a crucial part of the process.

The main contribution of this paper is to present a complete and adequate preliminary design of a mechanical differential and test bench, in the context of the parallel eAWD hybridization of a mid-size pickup truck. This topology is particularly interesting for the pickup segment, as the proposed 4x4 hybrid version can replace the existing

4x4 versions. In this case, components and packaging references from the existing rear differential can be utilized, eliminating the need for a driveshaft and a Diesel engine and contributing to the reduction of pollutant gas emissions. Moreover, his test bench can be assembled for this HEV develop and study project.

MECHANICAL DESIGN OF THE ELECTRIC POWERTRAIN

The mechanical design presented includes the sizing of all differential gears in accordance with the AGMA standard [12], as well as the sizing of the half-shaft, splines, and the selection of appropriate bearings for the system. The power input was defined based on a preliminary specification of the electric motor, which is the EMRAX 268 [14], as proposed in the study presented in [13], which outlines a preliminary hybridization design for a mid-size pickup truck. For simplification purposes, an open mechanical differential was considered. Later, the inclusion of a lockable system is valid to achieve better off-road capability.

GEARS SIZING - The sizing of the gears is divided between the sizing of the pinion and crown gear pair and the satellite and planetary gear pairs. These components are defined as shown in Figure 2. The input parameters are shown in Table 1.

Table 1 – Input parameters for the gears sizing [13].

Parameter	Symbol	Value
Module	m	5 mm
Quality number	Q_V	7
Pressure angle	φ	20°
Number of cycles (pinion)	c_i	10^7

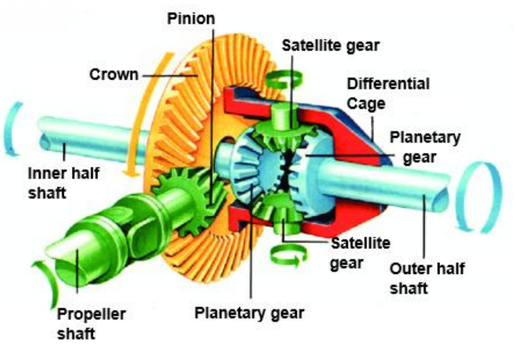

Figure 2 – Structure of a common vehicle mechanical differential. Adapted from [15].

Usually, calculations are performed for bending and wear. The safety factor for bending "S_F", is calculated as the ratio of the permissible bending stress "σ_{FP}" to the calculated bending stress "σ_F" (Equation 1). Similarly, the safety factor for wear "S_H" is found by dividing the permissible contact stress "σ_{HP}" by the calculated contact stress "σ_H" (Equation 2).

$$S_F = \frac{\sigma_{FP}}{\sigma_F} \tag{1}$$

$$S_H = \frac{\sigma_{HP}}{\sigma_H} \tag{2}$$

The acting stresses depend on the tangential force "W_t" (Equation 3) and on tabulated factors defined according to the AGMA standard [12], as well as specific parameters of each gear. The calculation for the bending and wear stresses of the gears is shown in Equation 4 and Equation 5, respectively.

$$W_t = \frac{P_{req}}{v_{et}} \tag{3}$$

$$\sigma_F = \frac{1000 \cdot W_t}{b} \cdot \frac{K_a \cdot K_v}{m} \cdot \frac{Y_x \cdot K_{HB}}{Y_B \cdot Y_J} \tag{4}$$

$$\sigma_H = Z_E \cdot \left[\frac{1000 \cdot W_t}{b \cdot d \cdot Z_I} \cdot K_a \cdot K_v \cdot K_{HB} \cdot Z_x \cdot Z_x c\right]^{1/2} \tag{5}$$

The allowable stresses, on the other hand, are related to the permissible stresses ("σ_{Hlim}" and "σ_{Flim}"), which vary according to the material and heat treatment, and also tabulated factors. All these values can be found in the AGMA standard [12]. The calculation for the permissible bending and wear stresses for the gears is shown in Equation 6 and Equation 7, respectively.

$$\sigma_{FP} = \frac{\sigma_{Flim} \cdot Y_{NT}}{K_\theta \cdot Y_z} \tag{6}$$

$$\sigma_{HP} = \frac{\sigma_{Hlim} \cdot Z_{NT} \cdot Z_W}{K_\theta \cdot Z_z} \tag{7}$$

Pinion and Crown - The sizing of the pinion and the crown gear began by defining the number of teeth for each component. Considering the desired reduction and the minimum number of 15 teeth for the pinion [16], the number of teeth for the pinion was determined as "$Z_p = 17$" and for the crown gear as "$Z_c = 76$", resulting in a reduction ratio of "$i_c = 4.4706$".

Regarding the material, it was selected the AISI 4140 carburized steel, surface-hardened grade 1, with a core hardness of 21 HRC and surface hardness of 55 HRC [17]. It is worth noting that the standard defines these values for steels compatible with the specified treatment, and medium-carbon steels (0.3% to 0.6%) meet this condition [18]. The entire sizing is based on spiral bevel gears. The initial calculated values are shown in Table 2.

Table 2 – Parameters for pinion and crown gears sizing [13].

Parameter	Symbol	Value
Required power (nominal)	P_{req}	117 kW
Primitive diameter of the pinion	d_p	85 mm
Primitive diameter of the crown	d_c	380 mm
Velocity in the primitive line	v_{et}	20.0 m/s
Primitive angle	γ	12.6°
Primitive angle	Γ	77.4°
Cone distance	A_0	194.7 mm
Face width	b	50 mm
Curvature radius	r_c	282.7 mm
Spiral average angle	ψ	35°

The output speed of the differential "n_s" is calculated according to Equation 8. The radius of curvature was determined using the software SolidWorks (Figure 3).

$$n_s = \frac{n_e}{i_c} = 1006.6 \text{ rpm} \tag{8}$$

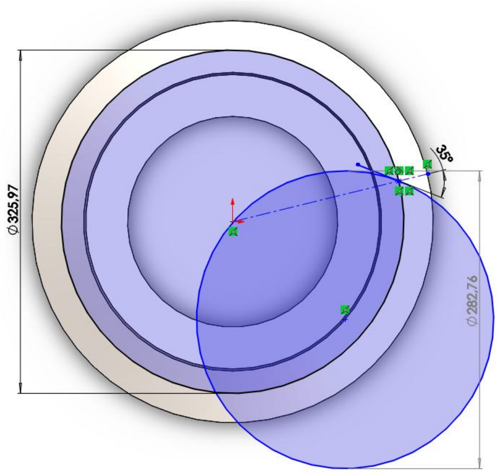

Figure 3 – Radius of curvature determination.

Finally, the safety factors for the bending and wear of the pinion and crown are determined:

$$S_{Fp} = 3.56$$

$$S_{Fc} = 3.81$$

$$S_{Hp} = 1.52$$

$$S_{Hc} = 1.67$$

For this case, the bending factors should be compared with the cube of the wear factors [19]. Through this comparison, it is possible to conclude that wear is a risk factor for the pinion, while bending is a risk factor for the crown.

Satellite and Planetary - The sizing of the other gears in the differential follows the same logic already presented. The main difference is that the bevel and planetary gears are straight-toothed bevel gears. An equal number of teeth was determined for both gears, with $z_s = z_{pl} = 30$. The selected steel was carburized and surface-hardened AISI 4140 grade 2, with a core hardness of 25 HRC and a surface hardness of 58 HRC [17]. The initial calculated values are shown in Table 3.

The safety factors for bending and wear of the satellite and planetary gears are determined:

$$S_{Fs} = S_{Fpl} = 1.93$$

$$S_{Hs} = S_{Hpl} = 1.39$$

For this case, the bending factors should be compared with the square of the wear factors [19]. Through this comparison, it is possible to conclude that wear is a risk factor for both gears.

Table 3 – Parameters for satellite and planetary gears sizing [13].

Parameter	Symbol	Values
Primitive diameter	$d_s = d_{pl}$	150 mm
Velocity in the primitive line	v_{et}	7.9 m/s
Primitive angle	γ	45°
Primitive angle	Γ	45°
Cone distance	A_0	106.1mm
Face width	b	50 mm

HALF SHAFT SIZING - A conventional automotive half shaft includes, in addition to the shaft itself, components such as constant-velocity joints, which allow the shaft to move and connect it to the wheel hub. Considering a simpler model that could be implemented on a test bench, it is used in this design a rigid shaft with a direct connection to the gears via splines. Suitable bearings for the application have also been selected.

Shaft Sizing - Regarding the dimensioning of a shaft, it is not necessary to evaluate stresses at every point, only at critical locations such as changes in diameter and notches, or in regions where the bending moment is more critical [19]. Therefore, it is necessary to create a free-body diagram of the component, considering the torque and bending moment along its length. To do this, it is essential to define the component's width as well as the arrangement of the bearings.

In the case of power transmission via gears, the analysis of the free-body diagram can be performed through separate calculations in two planes. The horizontal plane contains the tangential force, responsible for producing the torque. The vertical plane includes both the axial and tangential forces. It is worth noting that the axial force generates a moment related to the gear's pitch radius.

The analysis of a shaft involves combining different types of stresses into alternating and mean von Mises stresses (σ'_a and σ'_m). Regarding the acting stresses on the proposed half-shaft, it is defined that the electric motor operates with constant torques when required. Consequently, these stresses are identical and can be defined by Equation 9.

$$\sigma_a' = \sigma_m' = \sqrt{\left[\frac{16 \cdot K_f \cdot M_r}{\pi \cdot d^3} + \frac{2 \cdot K_{fa} \cdot W_a}{0{,}85 \cdot \pi \cdot d^2}\right]^2 + 3 \cdot \left[\frac{8 \cdot K_{fs} \cdot T}{\pi \cdot d^3}\right]^2} \quad (9)$$

Where "M_r" represents the resulting bending moment, "d" is the shaft diameter, "W_a" is the axial force, and "T" is the torque. Additionally, the factors for each type of stress can be defined using factor charts [19].

There are several differences between a practical application of a mechanical component and laboratory tests, such as manufacturing methods, stress concentrators, environmental conditions, and design. Therefore, Martin's equation (Equation 10) defines the relationship between the specimen's endurance limit (for most steels defined as half of the maximum allowable stress) and the endurance limit in the actual usage condition. Each factor represents a specific condition and is tabulated [19]. For this application, only the surface factor "K_a", size factor "K_b", and reliability factor "K_e" will be considered.

$$S_e = k_a \cdot k_b \cdot k_c \cdot k_d \cdot k_e \cdot k_f \cdot S_e' \quad (10)$$

First, the width of the shaft is defined by considering the distance from the gears to the center of the wheels (L_e = 753.1mm), which is based on the best-selling mid-size pickup truck in the Brazilian market in 2023, as considered in [13]. A shaft with a constant diameter of 55 mm was specified, made of cold-rolled AISI 1050 steel, which has a tensile strength limit "S_{ut} = 690 MPa" [19]. Both planes are defined as shown in Figure 4 and Figure 5, which also represents the arbitrated distance of the bearings and the forces acting on them.

From the contact of the gears, the tangential force (Equation 3), radial force (Equation 11), and axial force (Equation 12) are defined, as well as the torque (Equation 13) and the moment due to the axial force (Equation 14).

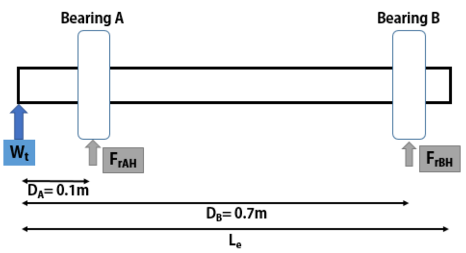

Figure 4 – Horizontal plane.

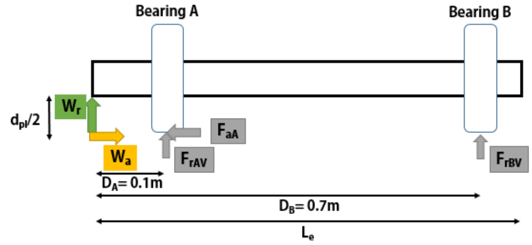

Figure 5 – Vertical Plane.

There are some online software tools available that can provide the support reactions and the equations for the bending moment along the shaft. The resulting bending moment at the critical point of the shaft was determined as M_r=1.48 kNm.

$$W_r = W_t \cdot \tan(\varphi) \cdot \cos(\tau) = 3.81 \text{ kN} \quad (11)$$

$$W_a = W_t \cdot \tan(\varphi) \cdot \sin(\tau) = 3{,}81 \text{ kN} \quad (12)$$

$$T = \frac{9550 \cdot P_{req}}{n_s} = 1109.9 \text{ Nm} \quad (13)$$

$$M_a = W_a \cdot \frac{d_{pl}}{2} = 285.7 \text{ Nm} \quad (14)$$

Given these parameters and all the indicated factors, a critical endurance limit of S_e = 189.9 MPa is obtained, and von Mises stresses of $\sigma'_a = \sigma'_m$ = 90.2 MPa. Finally, the Goodman fatigue criterion is considered, which results in a safety factor as indicated in Equation 15.

$$\frac{1}{n_f} = \frac{\sigma_a'}{S_e} + \frac{\sigma_m'}{S_{ut}} \therefore n_f = 1.59 \quad (15)$$

Splines Sizing - Splines are typically used for the transfer of high torques and are very common in automotive drive shafts, although they are more expensive to manufacture compared to keys. The sizing of splines can be performed similarly to that of cylindrical spur gears [20], to determine the torque capacity of the component and compare it with the torque applied to the shaft. Some of the main parameters are shown in Table 4.

Table 4 – Input parameters for the splines sizing.

Parameter	Symbol	Value
Primitive diameter	d_{best}	47.6 mm
Diametral pitch (chosen)	P_{dest}	1 mm^{-1}
Number of teeth	z_{est}	55
Effective teeth width	s_V	1.57 mm
External diameter	d_0	56 mm
Internal diameter	D_i	53.2 mm
Effective spline length (chosen)	L_{ef}	37.8 mm
Shear resistant area	A_τ	2828.2 mm^2
Contact area	A_{cd}	1440.4 mm^2

Finally, the torque capacity of the spline is calculated (Equation 16), which is directly proportional to the average shear stress on the shaft (Equation 17). The value obtained is approximately 2.7 times greater than the torque "T" calculated on the shaft. Therefore, the torque capacity of the spline is sufficient to meet the demand.

$$\tau_{med} = \frac{16 \cdot K_{fs} \cdot T}{\pi \cdot d^3} = 45.4 \text{ MPa} \tag{16}$$

$$M_{est} = 0.7854 \cdot D_{best}{}^2 \cdot L_{ef} \cdot \tau_{med} = 3.06 \text{ kNm} \tag{17}$$

Bearings Selection - Usually, only two bearings should support the components and withstand the loads. Furthermore, it is preferable to have just one bearing to support the axial load in order to allow greater tolerances in the shaft length dimensions and also to prevent binding in the event of shaft expansion [19]. Regarding the calculations required for bearing selection, the methodology adopted by SKF (2015) [21] is followed. Thus, the basic nominal life is defined according to Equation 18, in which the exponent "p" varies with the type of bearing and the equivalent dynamic load "P_{eq}" depends on the kind of load involved.

$$L_{10h} = \frac{10^6}{60 \cdot n_s} \cdot \left(\frac{C_d}{P_{eq}}\right)^p \tag{18}$$

For the selection of bearings, it is considered that the electric motor operates only with torques in the direction of moving the vehicle forward. Reverse is provided exclusively by the internal combustion engine. Therefore, bearing A is defined as a cylindrical roller bearing, and bearing B as a tapered roller bearing, so that it can support both radial and axial loads. Additionally, for automotive applications, the life of a bearing should exceed 69000 km [22]. Since this value is usually given in hours, for a single reduction ratio, the linear speed of the bearing "v_R" is calculated according to Equation 19. The bearing life in kilometers is given by the product of the linear speed and the life "L_{10h}" (Equation 20).

$$v_r = \frac{2 \cdot r_d \cdot \pi \cdot n_s \cdot 60}{1000} \tag{19}$$

$$L_{km} = L_{10h} \cdot V_r \tag{20}$$

The selected bearings were the SKF BS2-2211 for bearing A (spherical roller bearing) and the SKF P2BE55M-TRB-STHX for bearing B (tapered roller bearing). The main calculation data are presented in Table 5 and Table 6, respectively. The estimated life for both components is greater than the required.

Table 5 – Calculation parameters for bearing A.

Parameter	Symbol	Value
Static load	C_0	127 kN
Dynamic load	C_d	129 kN
Calculation factor	Y_0	2.8
Equivalent dynamic load	P_{eq}	17.7 kN
Bearing nominal life	L_{10h}	1970 h
Bearing linear velocity	v_R	12.66 m/s
Bearing life in km	L_{km}	$8.98 \cdot 10^4$

PRELIMINARY TEST BENCH DESIGN

The initial diagram of the proposed test bench is shown in Figure 6. The diagram is divided into mechanical, electrical, control, and hydraulic connections and includes a power source that would simulate vehicle loading. When an acceleration signal is sent to the ECU (Electronic Control Unit), it controls the inverter to drive the electric motor. Simultaneously, the BMS (Battery Management System) receives signals from the batteries, determining their state and whether more charge is needed in the system. All system status checks are performed through a supervisory system, which receives signals from the ECU and the BMS. Moreover, electric motors are coupled to each half-shaft, representing the load of the wheels. This choice is made to simplify the system, as the use of wheels would add more mass to the system and increase the complexity of the assembly. The focus of this work is on the mechanical part of the bench.

Table 6 – Calculation parameters for bearing B.

Parameter	Symbol	Value
Static load	C_0	186 kN
Dynamic load	C_d	151 kN
Calculation factor	Y_0	1.8
Equivalent dynamic load	P_{eq}	16.6 kN
Bearing nominal life	L_{10h}	4117 h
Bearing linear velocity	v_R	12.66 m/s
Bearing life in km	L_{km}	$1.88 \cdot 10^5$

The components selected for the system were the SKF 511-609 bearing box for bearing A and the SKFP2BE55M-TRB-STH for bearing B [23], as well as the FUTEK TRS605 torque transducer, whose operating torque is up to 500 Nm (maximum motor torque) and operating speed is up to 7000 rpm [24]. Regarding couplings, the HENFEL HXP 5.5 model was chosen to connect the motor to the differential (high speed), and the HENFEL HDF 220 coupling was selected to connect the half-shaft to the load motors (high speed) [25].

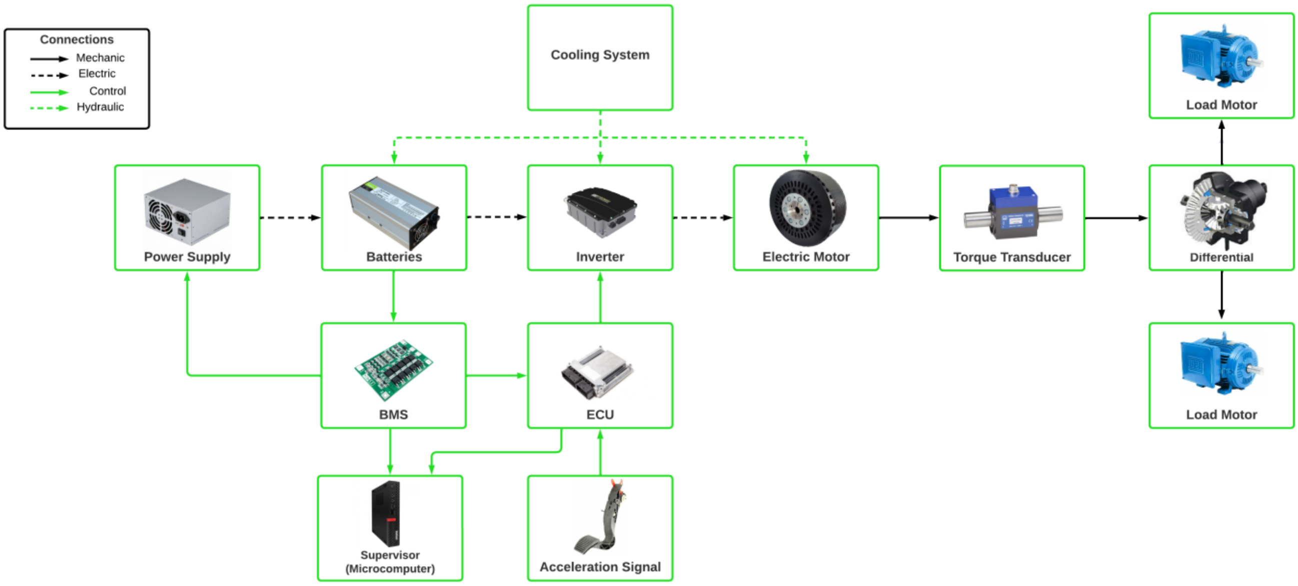

Figure 6 – Test bench diagram

TEST BENCH MODELING - In order to represent the bench components, the pinion, crown, and splined half-shafts were modeled in SolidWorks software. Satellite gears were obtained through the available Toolbox library. The bearings, transducer, and motor were sourced from the manufacturers online catalogs. For the elastic couplings, generic models obtained from the GrabCAD portal were considered. The base of the bench was repurposed from an existing bench in the Tesla Laboratory at UFMG (Universidade Federal de Minas Gerais). Additionally, the modeling of all the bases and supports for the components on the bench was carried out. The final result is shown in Figure 7.

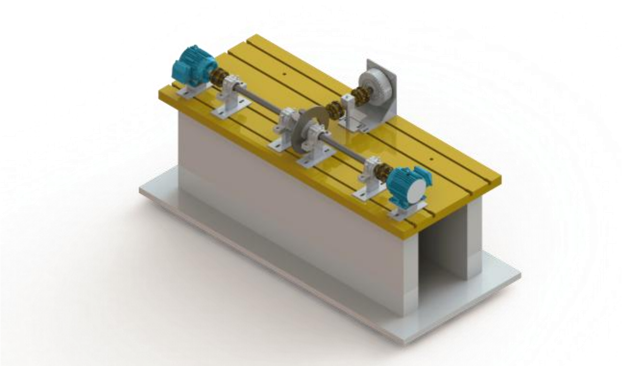

Figure 7 – Modeling of the mechanical part of the test bench.

PROPOSED TESTS - There are two main operating strategy functions that mot affect a HEV's fuel consumption: the control of the SOC (State of charge), and the decision to use electrical driving [11]. The main idea is to use the electric propulsion system during transient conditions, such as hill climbing and overtaking, for short durations. This approach ensures that the internal combustion engine (ICE) operates within its most efficient range.

To evaluate the system's performance, it is crucial to test the efficiency of the electric powertrain. Key aspects include acceleration and deceleration capabilities, thermal management of the motor and battery pack, and the charging/discharging processes. Thermal management performance should also be assessed. Additionally, validating the hybrid system’s control and software, including engine control logic and safety systems, is essential. Finally, Worldwide Harmonized Light Vehicles Test Procedure (WLTP) cycle tests can be conducted using hardware-in-the-loop (HIL) simulations to measure overall energy consumption and validate system performance under realistic driving conditions.

CONCLUSIONS

The preliminary mechanical design of a powertrain and a test bench for P4 hybrid electric pickups is proposed in this study. The design process included the dimensioning of differential gears according to AGMA standards, analysis of half shafts and splines, and the selection of appropriate bearings, ensuring robustness and reliability. Furthermore, the conceptual test bench design provides a versatile platform for simulating and evaluating the performance of the P4 hybrid electric vehicle under various control strategies. This work offers a practical tool for the optimization of components and control strategies in real-world scenarios. By enabling the manufacturing and validation of all system components, this study aims to support future developments in hybrid electric vehicle technology, contributing to the ongoing evolution of sustainable transportation solutions.

ACKNOWLEDGEMENTS

This study was financed in part by the Coordenação de Aperfeiçoamento de Pessoal de Nível Superior - Brasil (CAPES) - Finance Code 001.

REFERENCES

[1] Quatro Rodas. (2025). *Estes foram os 20 carros híbridos mais vendidos do Brasil em 2024*. https://quatrorodas.abril.com.br/carros-eletricos/estes-foram-os-20-carros-hibridos-mais-vendidos-do-brasil-em-2024 (Accessed: 6 March 2025)

[2] CNBC. (2024). *Hybrid car sales in India surge by 27 in 2024 as BEV growth slows, strong hybrids lead the way*. https://www.cnbctv18.com/auto/hybrid-car-sales-in-india-surge-by-27-in-2024-as-bev-growth-slows-strong-hybrids-lead-the-way-19468472.htm (Accessed: 6 March 2025)

[3] Poder 360. (2025). *BYD avança com obras de fábrica na Bahia e confirma produção em 2025*. https://www.poder360.com.br/poder-infra/byd-avanca-com-obras-de-fabrica-na-bahia-e-confirma-producao-em-2025/ (Accessed: 6 March 2025)

[4] Olhar Digital. (2024). *Fábrica da GWM já tem data para operar no Brasil*. https://olhardigital.com.br/2024/10/17/carros-e-tecnologia/fabrica-da-gwm-ja-tem-data-para-operar-no-brasil/ (Accessed: 6 March 2025)

[5] Ministério do Meio Ambiente. (2018). *Resolução N. 490, de 16 de novembro de 2018*. Governo Federal do Brasil. https://conama.mma.gov.br/?option=com_sisconama&task=arquivo.download&id=767 (Accessed: 22 October 2024)

[6] Kumaran, A., Emran, A., Rajan, R. S., Sharma, V., Sadekar, G., Laermann, M., Kötter, M., Lahey, H.-P., & Körfer, T. (2017). Affordable hybrid topology for PV and LDV's in prospering India: Case study of 48 V (P)HEV system benefits. In *2017 IEEE Transportation Electrification Conference (ITEC-India)* (pp. 1–6). https://doi.org/10.1109/ITEC-India.2017.8333824

[7] Gao, D. W., Mi, C., & Emadi, A. (2007). Modeling and Simulation of Electric and Hybrid Vehicles. *Proceedings of the IEEE, 95*(4), 729–745. https://doi.org/10.1109/JPROC.2006.890127115–132. https://doi.org/10.2516/ogst/2009064

[8] He, Y., Kwak, K. H., Kim, Y., Jung, D., Lee, J. H., & Ha, J. (2022). Real-Time Torque-Split Strategy for P0+P4 Mild Hybrid Vehicles With eAWD Capability. *IEEE Transactions on Transportation Electrification, 8*(1), 1401–1413. https://doi.org/10.1109/TTE.2021.3103149

[9] Verdonck, N., Chasse, A., Pognant-Gros, P., & Sciarretta, A. (2010). Automated Model Generation for Hybrid Vehicles Optimization and Control. *Oil and Gas Science and Technology, 65*(1),

[10] Zhao, H., Li, C., & Zhang, G. (2008). Design of a versatile test bench for hybrid electric vehicles. In *2008 IEEE Vehicle Power and Propulsion Conference*

[11] Sittig, A., Mumelter, G., & Rabenstein, F. (2011). Development and calibration of hybrid electric vehicle operating strategies using simulations and a hybrid power train test bench. In *2011 IEEE Vehicle Power and Propulsion Conference* (pp. 1–5). https://doi.org/10.1109/VPPC.2011.6043058

[12] ANSI/AGMA-2003-B97. (1997). *Rating the Pitting Resistance and Bending Strength of Generated Straight Bevel, Zerol Bevel and Spiral Bevel Gear Teeth*. Alexandria, Virginia: AGMA Standard.

[13] Gonçalves, A. S., & Scari, A. da S. (2025). Preliminary Hybridization Design of a Mid-Size Pickup Truck in the Brazilian Market with an Electric Motor Coupled to the Mechanical Differential on the Rear Axle. *The Journal of Engineering and Exact Sciences*, *11*(1), 21725. https://doi.org/10.18540/jcecvl11iss1pp21725

[14] EMRAX. (2020). *268 Datasheet*. Slovenia. https://emrax.com/wp-content/uploads/2024/02/EMRAX_268_datasheet_v1.5.pdf (Accessed: 26 March 2024)

[15] ResearchGate. (2015). *Structure of a common vehicle mechanical differential*. https://www.researchgate.net/figure/Structure-of-a-common-vehicle-mechanical-differential-Source_fig4_283779955 (Accessed: 27 August 2024)

[16] Almeida, J. (2020). *Capítulo 13 - Engrenagens Cônicas*. Curitiba: UFPR. http://ftp.demec.ufpr.br/disciplinas/TMEC038/Prof.Julio_Almeida/ELEMENTOS%20II%20-%20PERIODO%20ESPECIAL/Cap%EDtulo%2013%20Engrenagens%20C%F4nicas.pdf (Accessed: 22 October 2024)

[17] ANSI/AGMA-2001-D04. (2004). *Fundamental Rating Factors and Calculation Methods for Involute Spur and Helical Gear Teeth*. Alexandria, Virginia: AGMA Standard.

[18] Jones, L. (1986). *Selection of Material and Compatible Heat Treatments for Gearing*. *Gear Technology*. St. Louis, Missouri.

[19] Budynas, R., & Nisbett, J. K. (2011). *Shigley's Mechanical Engineering Design* (8th ed.). New York: McGraw-Hill.

[20] Lingaiah, K. (2002). *Machine Design Databook* (2nd ed.). McGraw-Hill.

[21] SKF. (2015). *Rolamentos de esferas*. SKF. https://rolamentoscbf.com.br/catalogo/SKF-Catalogo-Geral-Rolamentos.pdf (Accessed: 22 October 2024)

[22] da Silva, Scari A., Machado, G., & Leite, D. (2010). Transmission Bearings Optimization to Achieve Energy Efficiency. *SAE Technical Paper*. https://doi.org/10.4271/2010-36-0288

[23] SKF. (2019). *Caixas de mancal e unidades de rolamento*. SKF.

[24] Fueltek. (2024). *Model TRS605*. Fueltek.

[25] Henfel. (2024). *Acoplamentos Flexíveis*. Henfel.